IC2ML: Unified battery state-of-health, degradation trajectory and remaining useful life prediction via intra-cycle and inter-cycle enhanced

Journal of Power Sources 666 (2026) 239148

Contents lists available at ScienceDirect

Journal of Power Sources

journal homepage: www.elsevier.com/locate/jpowsour

IC^{2}ML: Unified battery state-of-health, degradation trajectory and remaining useful life prediction via intra-cycle and inter-cycle enhanced machine learning

Xinghao Huang [a,1], Chen Liang [a,1], Shengyu Tao [a,b,c,*], Yunhong Che [d], Ningyu Bian [a], Jiale Zhang [a], Runhua Wang [a], Yuqi Zhang [a], Bizhong Xia [a,**], Xuan Zhang [a,***]

[a] Tsinghua Shenzhen International Graduate School, Tsinghua University, Shenzhen, 518055, China
[b] Department of Civil and Environmental Engineering, UC Berkeley, Berkeley, CA, 94720, USA
[c] Department of Electrical Engineering, Chalmers University of Technology, Gothenburg, 41296, Sweden
[d] Department of Chemical Engineering, Massachusetts Institute of Technology, 02139, Cambridge, MA, USA

HIGHLIGHTS

- IC^{2}ML, a unified framework jointly predicting SOH, degradation trajectory, and RUL, is proposed.
- Health indicator are extracted from both 1-D voltage time series and 2-D images of voltage-capacity data.
- Spatiotemporal interaction among SOH, degradation trajectory and RUL is implemented through attention-based methods.
- The generalizability of IC^{2}ML is validated with batteries of 3 materials and 10 operating conditions.
- IC^{2}ML can adapt to limited data and extend to 100-cycle trajectory prediction with 1.77 % RMSE.

ARTICLE INFO

Keywords:
Lithium-ion batteries
State of health
Degradation trajectory
Remaining useful life
Machine learning

ABSTRACT

Strategic management of lithium-ion batteries (LIBs) depends on evaluating current health status and predicting future degradation paths. Despite extensive research on core management tasks like state of health (SOH) estimation, degradation trajectory prediction, and remaining useful life (RUL) prediction, these tasks remain isolated without leveraging their inherent connections. This work proposes an unified framework that enables joint battery SOH, degradation trajectory and RUL prediction via an intra-cycle and inter-cycle enhanced machine learning (IC^{2}ML). IC^{2}ML uses 1-D time-serials voltage data to implement SOH prediction, where inter-cycle embeddings are further self-attention for degradation trajectory prediction. The RUL is derived from degradation trajectory prediction based on anticipated SOH levels, enabled by cross attention between output embeddings and input inter-intra cycle embeddings. The results demonstrate that using 0.1V sampling interval data that can be extracted onsite, the average root mean square error for SOH, degradation trajectory, and RUL prediction is 1.85 %, 2.36 % and 23.90 cycles, respectively, validated on 121 batteries spanning 10 operation conditions. Sensitivity analysis shows that IC^{2}ML can be adapted to scenarios where a few historical data is accessible. Broadly, this work highlights the potential of strategical battery algorithm co-design using intra-cycle and inter-cycle battery degradation information for various management tasks.

* Corresponding author. Department of Civil and Environmental Engineering, UC Berkeley, Berkeley, CA, 94720, USA.
** Corresponding author.
*** Corresponding author.
E-mail addresses: shengyu.tao@chalmers.se (S. Tao), xiabz@sz.tsinghua.edu.cn (B. Xia), xuanzhang@sz.tsinghua.edu.cn (X. Zhang).
[1] Stands for the authors have equal contributions.

https://doi.org/10.1016/j.jpowsour.2025.239148
Received 1 August 2025; Received in revised form 4 November 2025; Accepted 17 December 2025
Available online 30 December 2025

1. Introduction

Lithium-ion batteries (LIBs), leveraging their high energy density and long duration advantages, have been deeply integrated into core fields such as electric vehicles [1], consumer electronics [2], and smart grids [3]. However, like most electromechanical systems, LIBs inevitably experience performance degradation during prolonged operation [4], especially under dynamic temperature and load conditions typical of electric vehicle and energy storage system applications, which manifests as capacity loss, reduced charging efficiency, and increased safety concerns [5]. Particularly in large-scale application scenarios such as new energy vehicles and energy storage power stations, even slight attenuation of battery performance may trigger future systemic risks [6,7]. Therefore, how to establish the evaluation of current health status and the prediction of future degradation paths through non-destructive methods has become a key link in ensuring the reliability and safety of energy systems [8,9].

Capacity fading, as a core indicator for measuring battery performance degradation, has always been the focus of industrial attention [10]. Whether it is the pursuit of high yield by battery manufacturers [11], the real-time monitoring needs of on-board battery management systems (BMS) [12], or the evaluation of echelon utilization by battery recycling enterprises, all revolve around maximizing the value of the battery life cycle under the premise of ensuring safety. Although the traditional full charge-discharge capacity test can intuitively reflect the current maximum available capacity of the battery, it is time-consuming [13] and cannot effectively predict the nonlinear degradation process caused by complex coupling mechanisms [14–17] such as impedance rise (IR), lithium inventory loss (LLI), and loss of active material (LAM), making it difficult to predict the future battery performance [18–20]. The method relying on destructive disassembly for evaluation is more direct, but this method causes additional damage to the battery itself [21,22]. How to perform rapid, non-destructive, and comprehensive health management of batteries remains a challenge[23–25].

In recent years, research work has focused on physics-based top-down models (such as equivalent circuit models or electrochemical state-space models) to characterize battery degradation by simulating voltage, current, and temperature behaviors for health management. However, these methods face challenges in terms of changes in different operating parameters and calibration of batteries [26,27]. Data-driven methods, including deep learning algorithms, can learn complex degradation model patterns and relationships from the statistical characteristics of data or in an end-to-end manner[28–31]. For example, in terms of state of health (SOH) estimation, some teams have achieved effective estimation of SOH based on arbitrary charging segments using the transformer architecture [32]. However, these approaches only evaluate the current health status while neglecting the prediction of future degradation paths. In the field of life prediction and degradation analysis, some studies have achieved high-precision degradation trajectory and life prediction by building physics-informed models based on initial manufacturing differences in early cycles [7], but they fail to validate their capability in full-lifecycle management. Based on these limitations, comprehensive management of a battery's current health status and future degradation through multi-task learning is regarded as a promising solution for effective battery health management [8,33]. Some research has established transferable models to simultaneously predict remaining useful life (RUL) and SOH based on capacity increment differences in partial cycles, but they ignore the degradation trajectory from the current SOH to the end of life, and treating RUL prediction as a downstream task of SOH prediction inherently has cumulative errors [34]. Some studies start from the correlation between RUL and SOH, and take RUL prediction as an auxiliary task for predicting degradation trajectories, but the maximum capacity of historical cycles required is often difficult to obtain in practical applications [35]. Even within the promising multi-task learning frameworks, these tasks remain isolated and fail to fully leverage their inherent connections. From a physical perspective, the current SOH point is the starting postion of future degradation trajectories, depending on the future operation conditions; while the RUL is the anticipated remaining time or cycles under defined end-of-life threshold of one of the degradation trajectories [36]. From a data perspective, data from different sampling points within the same cycle exhibit short-term degradation information, while performance changes between adjacent cycles contain key information about long-term degradation [14]. Recent advances have highlighted the significance of structured temporal modeling. The BatteryLife demonstrated that representing each charge-discharge cycle as an independent "token" and sequentially modeling intra-cycle and inter-cycle dependencies can effectively enhance life prediction performance [37]. Meanwhile, Some studies introducing inter-cell learning, capturing cross-cell correlations under heterogeneous ageing conditions to improve robustness and early-life prediction accuracy [38]. These studies have collectively validated the importance of hierarchical time-series representation and cell heterogeneity modeling for battery prognostics. Nevertheless, both approaches still focus primarily on single-task lifetime prediction, leaving the intrinsic relations among SOH, degradation trajectory, and RUL unexplored. The lack of integrated modeling that jointly consider the current health status and future degradation trajectories makes it difficult for models to capture the synergistic evolution of multi-dimensional health patterns during battery degradation.

This study proposes a unified framework enabling joint prediction of battery SOH, degradation trajectory, and RUL via intra-cycle and inter-cycle enhanced machine learning (IC^2ML). As shown in Fig. 1a, IC^2ML utilizes 1-D time-series voltage data sampled from random voltage intervals for SOH prediction, and combines self-attention mechanisms to capture inter-cycle differences for future degradation trajectory prediction. The RUL is defined as the result derived from degradation trajectory prediction and anticipated SOH levels within a future time horizon, implemented via a cross-attention mechanism between output embeddings of inter-cycle and intra-cycle embeddings of 2-D image data. This architecture effectively breaks the bottleneck of traditional methods in representational capability for intra-cycle 1-D spatial data, achieving spatiotemporal unified modeling of three health states during battery aging. As shown in Fig. 1b, the trained model can realize comprehensive health management throughout the entire lifecycle using only a small amount of easily accessible random samples from 0.1V voltage intervals. Validated on 121 batteries covering 10 operating conditions, the average RMSE for the SOH task is 2.08 %, with average RMSEs of 2.23 % and 55.69 cycles for degradation trajectory prediction and RUL prediction, respectively. Further sensitivity analysis demonstrates that IC^2ML can adapt to scenarios with limited historical data: when initialized with only the first 10 cycles of data, the average RMSE for RUL prediction is 65 cycles. Additionally, degradation trajectory prediction can be extended to 100 cycles with high precision, achieving an average RMSE of 2.20 %. Compared with state-of-the-art data-driven methods for batteries, IC^2ML achieves an average accuracy improvement of 21 % for SOH estimation tasks and 12 cycles for RUL prediction task. Overall, this study highlights the significant potential of strategically collaborative design of battery management algorithms using intra-cycle and inter-cycle battery degradation information, which can be applied to various management tasks such as SOH, degradation trajectory, and RUL prediction and beyond.

2. Dateset

This work employs three batches of batteries as case studies, with the batteries tested under different operating conditions, each batch undergoing testing throughout its full service life until the end of life (EOL). Batch 1 consists of $LiNi_{0.86}Co_{0.11}Al_{0.03}O_2$ positive electrode (NCA battery) with 3500mAh nominal capacity and cutoff voltages of 2.65–4.2 V.

Batch 2 contains $LiNi_{0.83}Co_{0.11}Mn_{0.07}O_2$ positive electrode (NCM

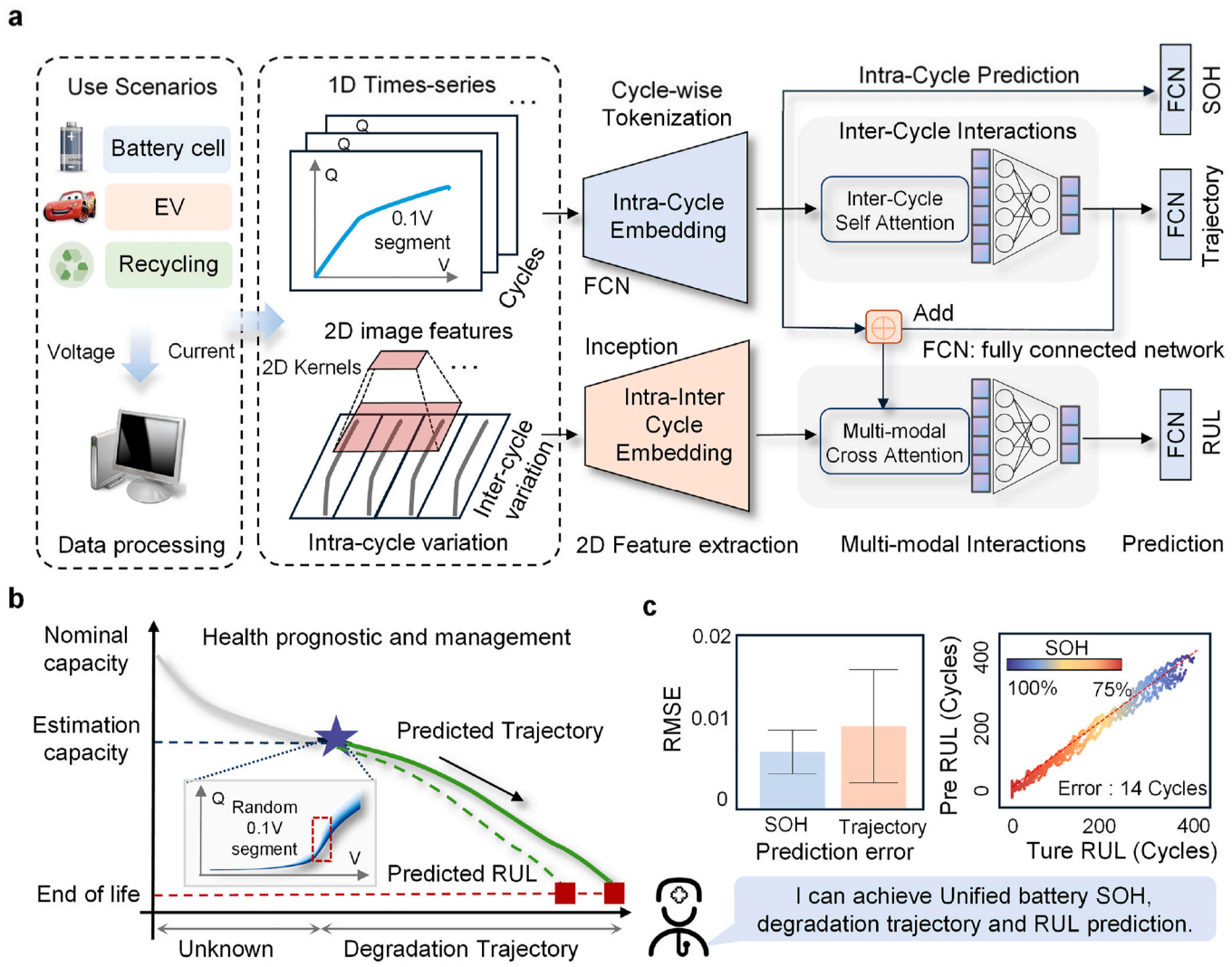

Fig. 1. Model architecture, deployment, and performance. (a) Data collected from multiple real-world scenarios are used for intra-cycle and inter-cycle modeling through 1-D time series and 2-D image features, respectively, to comprehensively manage multiple battery health tasks. **(b)** The trained model enables comprehensive health management using only a small amount of easily accessible data. **(c)** Performance examples of the model on three tasks.

battery) with 3500mAh nominal capacity and cutoff voltages of 2.5–4.2 V. Batch 3 includes 42 (3) wt.% $Li(NiCoMn)O_2$ blended with 58 (3) wt.% $Li(NiCoAl)O_2$ positive electrode (NCM + NCA battery) with 2500mAh nominal capacity and cutoff voltages of 2.5–4.2 V. All batteries were cycled in a thermal chamber under three temperatures (25 °C, 35 °C, and 45 °C) with variable charging rates (from 0.25C to 1C) and variable discharging rates (from 1C to 4C). Each battery underwent the same operating conditions throughout its lifecycle until reaching EOL (see Supplementary Table 1 for details). These datasets do not include cycling data under extreme conditions and are designed to simulate the requirements of EV application scenarios.

The degradation trajectories in Fig. 2a demonstrate the variability observed in cycling tests. Fig. 2b illustrates the relationship between initial capacity and RUL, Even with similar initial capacities, different batteries exhibit noticeable variations in RUL. This significant dispersion indicates that the battery degradation process is influenced by multiple coupled factors (such as manufacturing differences, operating conditions, and internal chemical non-uniformities), making RUL prediction a highly nonlinear, complex, and individualized task. Fig. 2c visualizes the two-dimensional image features of input data under selected segments. At different sampling time steps within a single cycle, varying capacity increase rates are observed due to distinct chemical reactions. Notably, significant differences also exist at the same sampling time steps across different cycles, which further underscores the effectiveness of collaborative modeling from both intra-cycle and inter-cycle perspectives. Fig. 2d presents the Pearson correlation between RUL and the maximum capacity of the current cycle across different materials and operating conditions, with correlations exceeding 90 % in all datasets. This indicates the interrelated nature of different health state characterizations.

3. Method

3.1. Intra cycle embedding and intra-inter cycle embedding

We normalize the data solely by dividing the capacity increment by the rated capacity to unify data dimensions, a method independent of sample size. Additionally, we perform intra-cycle embedding on the original capacity sampling sequence, treating each cycle's data as a token to learn the relationship between capacity increments at sampling points and battery aging:

$$X_{1D-embed} = Embed_{Intra}(X_{1D}) = LN(W_2\sigma(W_1X_{1D} + b_1) + b_2) \quad (1)$$

where, $X_{1D} \in \mathbb{R}^{10\times cycles}$, $W_1 \in \mathbb{R}^{d_{model}\times 10}$, $W_2 \in \mathbb{R}^{d_{model}\times d_{model}}$, $Embed_{Intra}$ represents the intra-cycle embedding. *LN* representation Layer nominalization. cycles represents the number of cycles in historical data, and

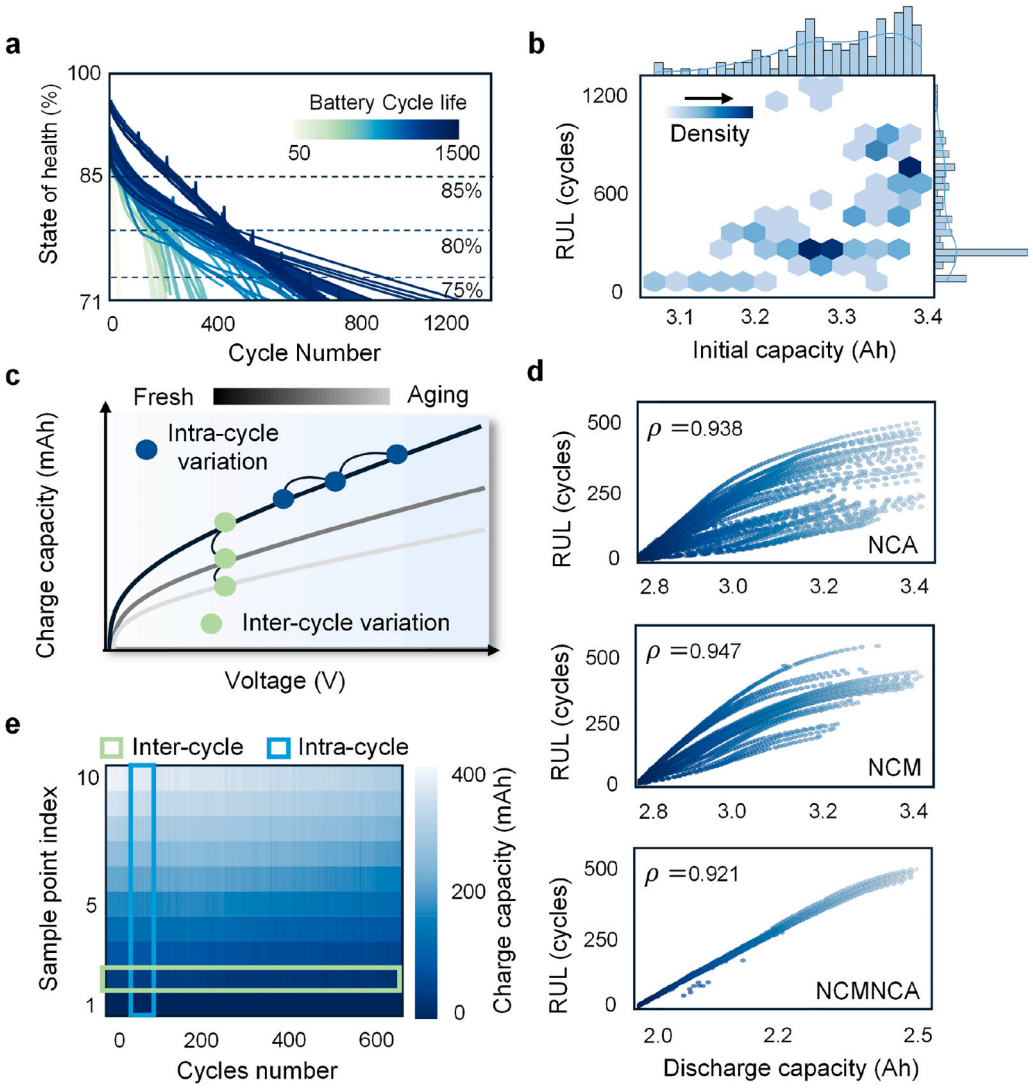

Fig. 2. Dataset Description. (a) Capacity degradation trajectories of the selected batteries. **(b)** Distribution relationship between initial capacity and RUL of the selected batteries. **(c)** Intra-cycle and inter-cycle differences during battery degradation. **(d)** Pearson correlation coefficient between current SOH and RUL. **(e)** Visualization of capacity curves in the selected interval reflecting battery degradation from a two-dimensional image perspective.

d_{model} represents the dimension of the hidden layer.

The temporal variations at each observation point exhibit two characteristic variation patterns: intra-cycle variations representing sequential changes between consecutive sampling points, and inter-cycle variations reflecting systematic differences at the same stage across different cycles. However, the original 1-D structure of the time series can only reflect changes between adjacent time points. We focus on 2D structure of time series that embodies battery aging. Such structures can present intra-cycle and inter-cycle variations, offering greater advantages in representational capacity. We treat the charging curves of historical cycles as 2D images, allowing intra-cycle and inter-cycle information to be extracted via 2D convolution.

$$X_{2D-embed} = Embed_{inter-intra}(X_{2D}) = LN(W_4 Inception(X_{2D}) + b_4) \tag{2}$$

where, $X_{2D} \in \mathbb{R}^{1\times cycles\times 10}$, and for $Embed_{inter-intra}$, we adopt the classic Inception block from the computer vision (CV) domain to demonstrate the universality of this approach and process the 2D tensor [39], $W_4 \in \mathbb{R}^{d_{model}\times 128}$.

3.2. Inter-cycle self-attention

Battery degradation trajectories are influenced by multiple coupled aging modes, leading to variations both within cycles and at corresponding sampling time steps across cycles. After intra-cycle embedding, we employ an inter-cycle self-attention mechanism to capture aging disparities during different battery cycles. By modeling the temporal dependencies in the cycle sequence, this mechanism effectively extracts long-term degradation features and adaptively focuses on critical cycles that significantly impact future battery degradation. First, positional encoding is applied to each embedded cycle:

$$PE(pos, 2i) = \sin\left(\frac{pos}{10000^{\frac{2i}{d_{model}}}}\right) \tag{3}$$

$$PE(pos, 2i+1) = \cos\left(\frac{pos}{10000^{\frac{2i}{d_{model}}}}\right) \tag{4}$$

where pos is the position vector, and i is the cycle index.

$$Attention(Q, K, V) = softmax\left(\frac{QK^T}{\sqrt{d_{model}}}\right)V \tag{5}$$

In the self attention mechanism, K, Q, V represent $key(K)$, $query(Q)$ and $value(V)$, respectively, and d_{model} denotes the input dimension

$$X_{IA} = Inter-cycle\ attention(X_{1D-embed}) = W_3 \cdot flatten(LN(X_{1D-embed} + Self\ Attention(X_{1D-embed} + PE))) + b_3 \quad (6)$$

We apply an Inter-cycle self-attention mechanism to the vectors after intra-cycle embedding to model relationships between cycles,. Following a residual network, the flattened vector of each cycle is mapped to the hidden dimension d_{model} via a fully connected layer $W_3 \in \mathbb{R}^{cycles \cdot d_{model} \times d_{model}}$.

3.3. Multi-modal cross-attention

Modeling battery aging with 1-D time series and 2-D image features offers different dimensions and information granularity. We employ a cross-attention mechanism to bridge these two modalities. We enable interaction between the self-attention-modeled vectors of each cycle and the embedded image feature vectors.

$$\begin{aligned} X_{MMA} &= Multi-modal\ Attention(X_{2D-embed}, X_{IA}) \\ &= Cross\ Attention(X_{2D-embed}, X_{IA}) \end{aligned} \quad (7)$$

3.4. Multi-task learning for comprehensive battery health management

We model comprehensive and in-depth battery aging information through multi-modal intra-cycle and inter-cycle analysis.For single-cycle SOH estimation, we directly estimate SOH from the intra-cycle embedded vectors.

$$Y_{SOH} = W_{SOH} X_{1D-embed} + b_{SOH} \quad (8)$$

For SOH estimation, we use a linear transformation $W_{SOH} \in \mathbb{R}^{1 \times d_{model}}$. For future degradation trajectory prediction, we leverage the vectors obtained from intra-cycle embedding and inter-cycle self-attention applied to 1-D time series.

$$Y_{Tra} = W_{Tra} X_{IA} + b_{Tra} \quad (9)$$

where $W_{Tra} \in \mathbb{R}^{horizon \times d_{model}}$, with "horizon" denoting the prediction length of the degradation trajectory. For RUL prediction, we use the vectors processed by combining the two modal inputs for prediction.

$$Y_{RUL} = W_{RUL} X_{MMA} + b_{RUL} \quad (10)$$

where, $W_{RUL} \in \mathbb{R}^{1 \times d_{model}}$. During the training process, these three prediction subtasks are optimized simultaneously, and the loss function consists of the following three components:

$$Loss_{SOH} = \frac{1}{N} \sum_{i=1}^{N} \left\| \widehat{Y^i_{SOH}} - Y^i_{SOH} \right\|^2 \quad (11)$$

$$Loss_{Tra} = \frac{1}{N} \sum_{i=1}^{N} \left\| \widehat{Y^i_{Tra}} - Y^i_{Tra} \right\|^2 \quad (12)$$

$$Loss_{RUL} = \frac{1}{N} \sum_{i=1}^{N} \left\| \widehat{Y^i_{RUL}} - Y^i_{RUL} \right\|^2 \quad (13)$$

$$Loss = \alpha Loss_{SOH} + \beta Loss_{Tra} + \gamma Loss_{RUL} \quad (14)$$

We set $\alpha = 1$, $\beta = 1$, $\gamma = 0.5$ for experiments, though other hyper-parameter may yield better results.

4. Result and analysis

4.1. Model performance and generalization capability

This section aims to demonstrate the effectiveness of the proposed method from multiple dimensions. As shown in Fig. 3a, we visualize the results of one experiment out of ten. It can be observed that the proposed method exhibits superior performance in real-time SOH estimation across three battery materials under different operating conditions. The average RMSE for the three materials is 1.82 %, with a standard deviation of 1.69 %. Moreover, the estimation performance on the NCMNCA dataset is more stable, with the maximum RMSE not exceeding 6.93 %. This level of accuracy is achieved merely based on a 0.1V sampling segment. For the NCA dataset, he overall RMSE is relatively large at 2.28 %, the RMSE of some samples reaches 8.75 %, which may be attributed to significant sampling errors in the data itself.

Fig. 3b presents the RUL prediction results across different datasets. We randomly selected one experimental result from ten trials involving three materials and four operating conditions for case analysis, with the complete results provided in Supplementary Figs. 5–7. It is evident that the best performance is achieved on the NCMNCA dataset, with an average error of only 5 cycles. This can be attributed, on one hand, to the effective long-term temporal modeling of battery aging data by the proposed method, and on the other hand, to the more linear degradation trajectory of the NCMNCA dataset compared to others, which simplifies the prediction task. In contrast, the prediction performance on the NCA dataset is relatively poorer, with an average error of 60 cycles. As shown in Fig. 2b, cells with similar initial capacities may follow markedly different degradation paths, resulting in broader distribution spread and more pronounced nonlinearity in later stages. This increases the intrinsic uncertainty of long-horizon RUL prediction, especially when future degradation trajectories diverge significantly under similar initial states. Furthermore, the NCA cells demonstrate more evident inflection points and local fluctuations in their degradation curves, introducing higher temporal non-stationarity that challenges sequence-based prediction models.

Fig. 3c illustrates the prediction results of the three tasks during the early, middle, and late stages of degradation. For the RUL prediction task, the errors for the three materials in the early and late stages are 35, 44, 13 and 6, 25,10 cycles respectively, with significantly higher accuracy in the late stage than in the early stage. This indicates that batteries with different RULs do not exhibit substantial performance differences in the early manufacturing stage. Additionally, the lower prediction accuracy for NCM batteries highlights the challenges of prediction based on extremely limited historical cycles and sampling intervals. For the SOH prediction task, the accuracy remains stable across the early, middle, and late stages for all three materials, with average errors of 2.23 %, 1.50 %, and 2.22 % respectively. Given that only a 0.1V sampling interval is used, this accuracy meets the requirements of most practical applications. For the degradation trajectory prediction task: For NCA batteries, larger discrepancies are observed in the early stage, with a RMSE of 2.27 % and a standard deviation of 1.65 %, while the middle stage shows higher accuracy (RMSE: 1.72 %, standard deviation: 1.87 %), which may be related to the degradation inflection points focused on in many existing studies. For NCM batteries, larger errors appear in the early stage, with an average RMSE of 3.03 % and a standard deviation of 2.60 %. For NCMNCA batteries, stable performance is observed in the early and middle stages (average RMSE: 1.79 % and

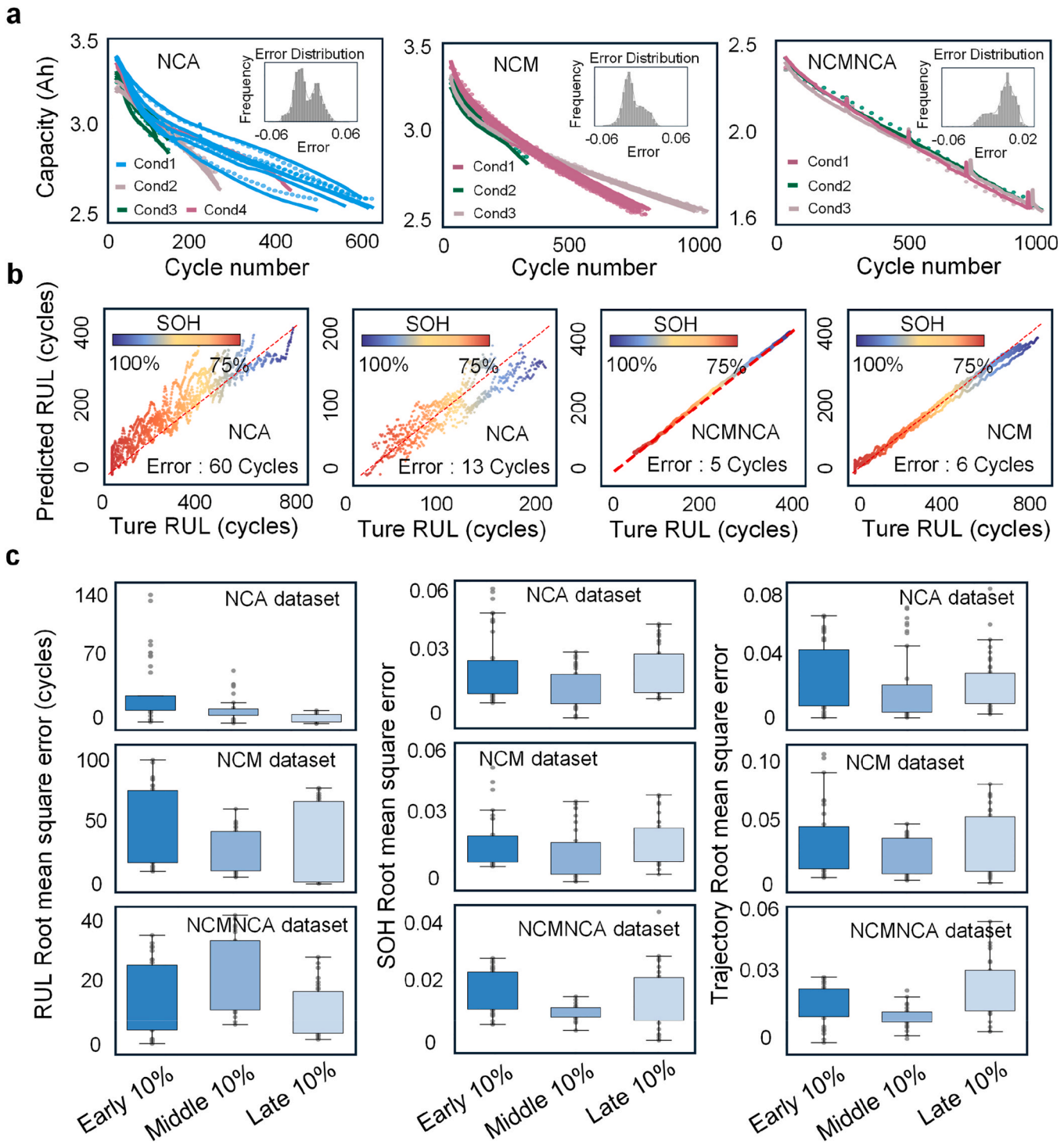

Fig. 3. Results and analysis. **(a)** SOH prediction results of the model on three datasets. **(b)** RUL prediction results under partial operating conditions. **(c)** Performance analysis of the three tasks at different lifecycle stages.

1.24 % respectively), while a larger error occurs in the middle-late stage (average RMSE: 2.45 %, standard deviation: 1.08 %).

Fig. 4a, b, and c show the results of ablating different modules of the proposed method to investigate their contributions to the prediction outcomes. Specifically, two ablation experiments were conducted: 1) Removing the one-dimensional time series input and using only two-dimensional images for multiple prediction tasks; 2) Removing the two-dimensional image feature input and using only one-dimensional time series for multiple prediction tasks. Detailed ablation experiments are provided in Supplementary Note 4.

In the SOH estimation task, it can be observed that in all three datasets, the prediction errors after removing the one-dimensional time series module are relatively larger, at 3.38 %, 4.82 %, and 2.87 % respectively. This indicates that for the capacity prediction task, intra-cycle modeling contains richer information compared to inter-cycle modeling relationships. Using only 2-D image features as input weakens the ability to learn intra-cycle information to some extent, leading to a decline in the SOH prediction performance for the current cycle.

For the RUL prediction task, the removal of the 2D image module in

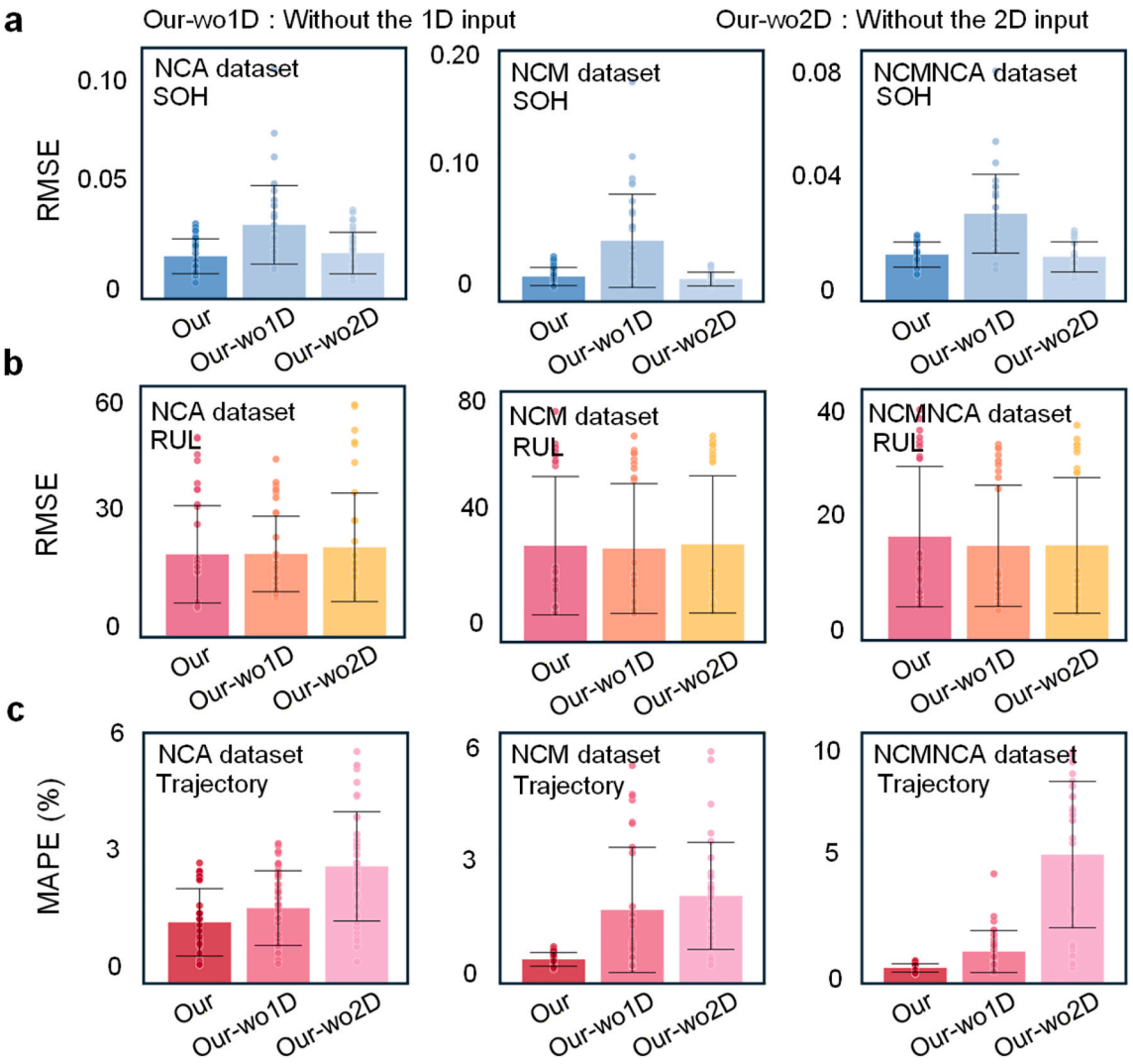

Fig. 4. Ablation experiments. **(a)** Performance analysis of SOH estimation on three datasets. **(b)** Performance analysis of RUL prediction on three datasets. **(c)** Performance analysis of degradation trajectory prediction on three datasets. two ablation experiments were conducted, Our-wo1D:Removing the one-dimensional time series input and using only two-dimensional images for multiple prediction tasks, Our-wo2D:Removing the two-dimensional image feature input and using only one-dimensional time series for multiple prediction tasks.

the NCA dataset significantly affected the model performance. The average RMSE of the prediction error increased from 19.38 cycles (with a standard deviation of 11.60) in the original model to 21.06 cycles (with a standard deviation of 12.95). In contrast, an interesting phenomenon was observed for the NCMNCA dataset, where both ablation schemes led to slightly improved performance, with the average RMSEs of the three models being 15.28 %, 13.92 %, and 13.99 %, respectively. This outcome stems from the inherent linearity of the degradation trajectories in the NCMNCA cells, where the capacity fading follows a near-linear trend throughout the lifetime. In such cases, the prediction task becomes relatively straightforward, and introducing more complex spatiotemporal modules may introduce redundant representations or amplify minor noise components, resulting in marginally degraded performance. Therefore, the reduced gap between the full and ablated models does not indicate the insignificance of the intra- or inter-cycle features, but rather reflects the data distribution characteristics of NCMNCA batteries. Under more nonlinear degradation behaviors, as observed in the NCA and NCM datasets, the full IC2ML framework demonstrates clear advantages, confirming the necessity of jointly modeling intra- and inter-cycle information for comprehensive health management.

In the trajectory prediction task, both ablation schemes demonstrated significant performance degradation across the three datasets. In the NCA dataset, the average MAPE increased from 1.24 % to 1.53 % and 2.39 % respectively; in the NCM dataset, the average RMSE rose from 0.55 % to 1.72 % and 2.06 % respectively. This further validates the effectiveness of the proposed scheme.degraded after ablation. For the NCA dataset, the average MAPE increased from 1.21 % to 1.81 % and 1.79 % respectively; for the NCM dataset, the average RMSE increased from 0.74 % to 1.61 % and 1.60 % respectively. These results further demonstrate the effectiveness of the proposed scheme.

4.2. Uncertainty analysis

This section aims to investigate the uncertainty of the model and its sensitivity to relevant hyperparameters. As shown in Fig. 5a, we compared two models: CRNN [34], which had been proven to exhibit superior performance, and BiLSTM, a commonly used model in the field of temporal modeling. We used NCM batteries as a case study, and the results are shown in Table 2. In the capacity prediction task, the average MAE of the three models (including our proposed model) was 1.67 %, 1.86 %, and 2.48 % respectively. For the BiLSTM model, some samples showed an estimation error exceeding 5.00 %. In the degradation trajectory prediction task, the average MAE of the three models was 1.53

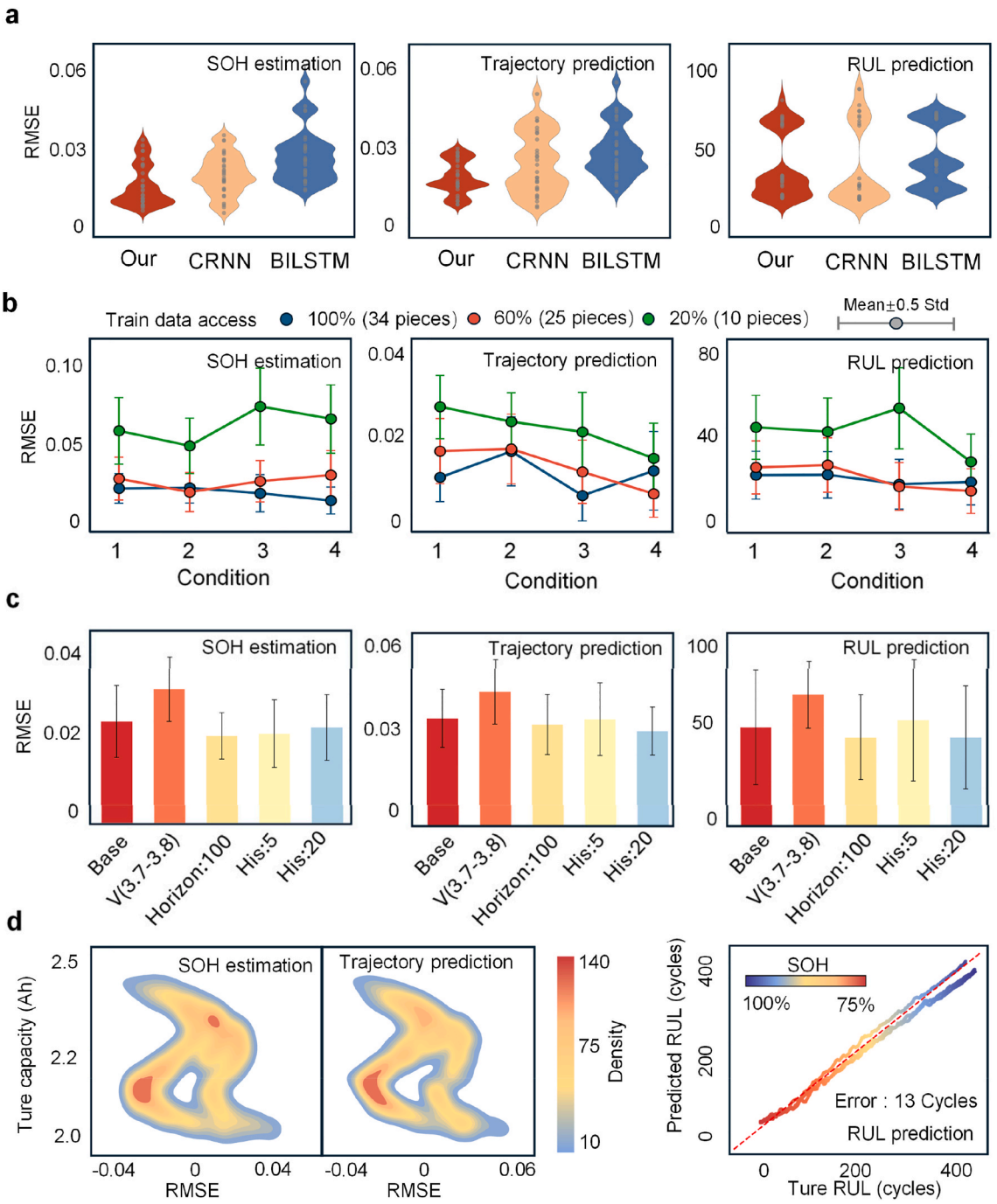

Fig. 5. Uncertainty analysis. **(a)** Performance comparison with current popular models. **(b)** Correlation analysis between training data volume and model performance. **(c)** Impact of different hyperparameters on model performance. **(d)** Prediction results cross-operation-condition.

%, 1.90 %, and 2.21 % with standard deviations of 0.44 %, 0.77 %, and 0.68 % respectively. Our model achieved the most stable and effective prediction results, indicating its effectiveness in temporal modeling. For the RUL prediction task, there was no significant difference among the three models, with average MAEs of 23.50, 29.47, and 35.31 cycles respectively, demonstrating the effectiveness of the selected model in temporal modeling, but its poor performance in the other two tasks highlights the challenges of comprehensive health management throughout the entire lifecycle. Meanwhile, we employed three models including Transformer, CNN, and GRU for separate single-task learning. It was observed that Transformer exhibited a relatively large error in the SOH estimation task, which might be attributed to insufficient training data. In contrast, GRU performed relatively well in the degradation

Table 1
Literature review of existing approaches.

References	SOH	Trajectory	RUL	Inter-intra cycles	inter-cell	Task collaboration
[32]	✓					
[7]		✓	✓			
[34]	✓		✓			✓
[37]			✓	✓		
[35]		✓	✓			✓
[38]			✓			
IC^{2}ML	✓	✓	✓	✓		✓

Table 2
The summary of estimation errors for the NCM dataset using various methods.

Method	State of health		Degradation trajectory		Remaining useful life	
	RMSE (%)	MAE (%)	MAPE	MAE (%)	RMSE (cycles)	MAE (cycles)
Our	**1.75**	**1.66**	**0.55**	**1.53**	30	23
Our (wo1D)	4.81	4.35	1.61	4.58	**29**	24
Our (wo2D)	1.80	1.51	1.60	4.57	30	25
CRNN	2.38	1.86	0.67	1.90	30	**22**
BILSTM	3.01	2.48	0.79	2.21	35	29
Transformer	2.23	1.82	\	\	\	\
GRU	\		0.70	1.99		\
CNN	\	\		\	44	32

trajectory prediction task, reflecting the strong temporal dependencies inherent in battery aging.The detailed results obtained using different methods are presented in Table 1.

Fig. 5b presents an analysis of the proposed method's robustness under limited training data. For the SOH estimation task, when 100 %, 60 %, and 20 % of the training data were used, the average RMSEs were 1.96 %, 2.12 %, and 2.96 %, respectively, with standard deviations of 0.79 %, 1.08 %, and 1.70 %. Notably, reducing the training data did not always degrade estimation accuracy; in certain operating conditions, the model trained with 60 % of the data even outperformed the one trained with 100 %. This indicates that SOH estimation relies less heavily on large data volumes, as it depends more on local degradation representations than long-term dynamics. For the degradation trajectory prediction task, with 100 %, 60 %, and 20 % of the training data, the average RMSEs were 4.56 %, 4.61 %, and 6.14 %, respectively, with standard deviations of 2.67 %, 2.85 %, and 3.87 %. As expected, both accuracy and robustness improved with more training data, and a notable decline occurred when the available data dropped to 20 %. For the RUL prediction task, the average RMSEs were 19.34, 20.19, and 24.21 cycles, respectively, with standard deviations of 11.60, 11.46, and 12.57 cycles. Interestingly, there was little difference in accuracy between using 60 % and 100 % of the data, which diverges from the trends in the other tasks. This observation primarily stems from the inherent cell-to-cell variability of the RUL task, even under identical materials and operating conditions, degradation trajectories differ substantially across cells. When training data are reduced, the retained subset may occasionally share higher distributional similarity with the test set, resulting in comparable or slightly better performance. However, for large-scale battery prognostics models encompassing a broader data distribution, a reduction in training data is expected to lead to a clear and monotonic decline in prediction accuracy.

This insight highlights the need for future work to explicitly model inter-cell variability to enhance generalization across heterogeneous battery populations. Fig. 5c analyzes the impact of changes in different hyperparameters on model accuracy, specifically examining three aspects: the availability of historical data, the length of predicted future degradation trajectories, and the influence of different sampling intervals. The Base model uses 10 historical cycles with voltage samples in the 3.6-3.7 V range, while predicting the degradation trajectory, SOH, and RUL for the next 50 cycles. It should be noted that only one variable was changed at a time to ensure the rigor of the experimental results. In the capacity prediction task, changing the sampling voltage interval led to a noticeable performance decline, with the average RMSE increasing from 2.00 % to 2.65 %. This may be because the 3.7-3.8 V interval is closer to the incremental capacity (IC) peak, and the influence of the IC peak on the capacity curve reduces the accuracy of SOH estimation.

Regarding the extension of the predicted degradation trajectory, no significant performance changes were observed, with all three tasks showing slight improvements. Specifically, the RUL prediction error decreased to 30.92 cycles, indicating the interrelatedness of health tasks, longer prediction lengths may enhance RUL prediction performance, consistent with observations from other studies.

For the availability of historical data, increasing the length of accessible historical data significantly improved the performance of RUL and degradation trajectory prediction, with average RMSEs decreasing to 30.95 cycles (standard deviation: 18.02) and 1.66 % (standard deviation: 0.42 %) respectively. Conversely, reducing the length of historical data increased the RUL prediction error from 34.42 to 36.96 cycles. These results confirm a positive correlation between the availability of historical data, RUL prediction length, and the accuracy of degradation trajectory prediction. Compared to other studies with strict data requirements, our method achieves superior performance using only 5 cycles of data within a 0.1 V sampling interval.

In Fig. 5d, we analyzed the model's capability for cross-condition prediction. Specifically, we mixed data from different operating conditions of NCMNCA material batteries for simultaneous training and prediction. In the SOH prediction task, the average RMSE was 1.67 % with a standard deviation of 1.63 %. In the degradation trajectory prediction task, the average RMSE was 1.82 % with a standard deviation of 1.72 %, and the average RUL prediction was 13.26 cycles. This indicates that the proposed method has good generalization ability and can learn the charging differences caused by different operating conditions. Additionally, we present the prediction results of simultaneous cross-material and cross-condition scenarios in Supplementary Fig. 8, further demonstrating the potential of the proposed method to become a pre-trained unified battery management large model in the future.

5. Discussion

Existing health management methods overlook the inherent connections among various battery management tasks such as SOH estimation, degradation trajectory prediction, and RUL prediction, thus treating each task isolated. The degradation trajectory is initially anchored at the current SOH status, and its path directly determines the magnitude of RUL given an end-of-life threshold. The absence of integrated models that simultaneously account for current health status and future degradation trajectories hinders the ability to capture coupled evolution of multi-dimensional health indicators throughout battery aging. This study proposes a unified framework to establish connections among these health management tasks, which can leverage accessible data from BMS to realize joint prediction of battery SOH, degradation trajectory, and RUL via intra-cycle and inter-cycle enhanced machine learning, which is named as IC^2ML in this paper.

Comprehensive effectiveness evaluations were conducted on datasets of 120 batteries with 3 different materials, including NCA, NCA, and NMCNCA. The proposed method achieves RMSE of 1.85 % for SOH estimation, 2.36 % for degradation trajectory prediction, and 23.90 cycles for RUL prediction across the three key battery management tasks. Thanks to the IC^2ML, the required historical data can be reduced to only 5 cycles to make future predictions, with the RMSE of degradation prediction being 1.87 %. Meanwhile, based on effective time-series modeling, the prediction length can be extended to a time horizon of 100 cycles, with a RMSE of 1.77 % and a maximum RMSE lower than 3.45 %. Comparisons with current experimental results of battery multi-health task prediction and single-task prediction models reflect the advantages of this hierarchical collaborative management. The generalization ability of the model was verified under the a simulated data scarcity condition where the ratio of training data to test data was 2:3. The robustness of the model was confirmed through hyperparameter sensitivity analysis.

The method proposed in this paper breaks the fragmented situation of various tasks in traditional health management and provides a more efficient, accurate, and comprehensive paradigm by integrating the hierarchical dependencies of multiple tasks. However, it should be acknowledged that this work only conducts health management tasks based on electrochemical characteristics, and domain knowledge has not been incorporated into the modeling. As the next step, clear physical

knowledge can be integrated into the data-driven model to improve self-interpretability [40], such as dQdV peaks [41], so as to establish physics-informed dependencies between different health management tasks. Random initial SOC is an important factor to consider in relation to the availability of field data. Although the effectiveness of the proposed method has been validated under random 0.1 V voltage segments, different voltage intervals involve complex electrochemical reactions. In addition, LFP batteries exhibit a plateau effect in their charging curves. Future work could consider incorporating an SOC-aware mechanism during the feature extraction phase to better address battery degradation under different SOC conditions. We also acknowledge that the current experiments do not cover extreme temperatures or high-rate conditions. Future work will extend the operating range to further verify the model's robustness and adaptability, as well as provide deeper insights into temperature- and rate-dependent degradation behaviors. In addition, it is necessary to further analyze the uncertainty of future degradation trajectories under highly random and time-varying working conditions, especially to establish an evaluation system with statistical confidence intervals, and simultaneously evaluate degradation mechanisms under extreme or special operating conditions through physical modeling to ensure the safe and long-term operation [4]. Future work will focus on non-invasive in-situ sensing signals [42] (such as vibration sensing, strain sensing, ultrasonic signals, and optical fiber sensing) to enhance the observation of internal states. Although existing methods have established a connection between the current health status of individual cells and their future degradation trajectories, enabling comprehensive lifecycle management, significant variations in degradation paths can still be observed among batteries with identical materials and capacities due to initial manufacturing differences and other factors. Future work could incorporate contrastive learning and related techniques to explicitly model inter-cell [38] variability for more accurate prediction. Meanwhile, in practical applications, there are inconsistencies among individual cells in the battery pack. These differences between cells will intensify with the increase of cycle times, thereby affecting the health status and service life of the entire battery pack [36]. Future work can construct a health management model that collaborates between individual cells and the pack to achieve accurate evaluation and effective management of the overall health status of the battery pack.

In brief, this study highlights the significant potential of the strategical co-design of battery management algorithms using intra-cycle and inter-cycle battery degradation information using the proposed IC^{2}ML framework, which can be applied to various battery health management tasks such as SOH, degradation trajectory, and RUL prediction and beyond.

CRediT authorship contribution statement

Xinghao Huang: Visualization, Validation, Software, Formal analysis, Data curation, Conceptualization. **Chen Liang:** Visualization, Validation, Software, Conceptualization. **Shengyu Tao:** Visualization, Validation, Supervision, Software, Conceptualization. **Yunhong Che:** Validation, Supervision. **Ningyu Bian:** Conceptualization. **Jiale Zhang:** Software, Conceptualization. **Runhua Wang:** Validation. **Yuqi Zhang:** Writing – review & editing. **Bizhong Xia:** Validation, Funding acquisition. **Xuan Zhang:** Funding acquisition, Formal analysis.

Declaration of competing interest

The authors declare that they have no known competing financial interests or personal relationships that could have appeared to influence the work reported in this paper.

Acknowledgments

This work was funded by the National Natural Science Foundation of China (Grant No. 51877120), the Key Scientific Research Support Project of Shanxi Energy Internet Research Institute (No. SXEI2023A002), and the Meituan Scholar Program-International Collaboration Project (No. 202209A).

Appendix A. Supplementary data

Supplementary data to this article can be found online at https://doi.org/10.1016/j.jpowsour.2025.239148.

Data availability

The data and code for this work has been deposited at https://github.com/terencetaothucb/IC2ML-Unified-battery-health-prognostics-via-intra-and-inter-cycle-enhanced-machine-learning.

References

[1] P.M. Attia, A. Grover, N. Jin, K.A. Severson, T.M. Markov, Y.-H. Liao, M.H. Chen, B. Cheong, N. Perkins, Z. Yang, P.K. Herring, M. Aykol, S.J. Harris, R.D. Braatz, S. Ermon, W.C. Chueh, Closed-loop optimization of fast-charging protocols for batteries with machine learning, Nature 578 (2020) 397–402, https://doi.org/10.1038/s41586-020-1994-5.

[2] A. Innocenti, S. Beringer, S. Passerini, Cost and performance analysis as a valuable tool for battery material research, Nat. Rev. Mater. 9 (2024) 347–357, https://doi.org/10.1038/s41578-024-00657-2.

[3] J. Figgener, J. Van Ouwerkerk, D. Haberschusz, J. Bors, P. Woerner, M. Mennekes, F. Hildenbrand, C. Hecht, K.-P. Kairies, O. Wessels, D.U. Sauer, Multi-year field measurements of home storage systems and their use in capacity estimation, Nat. Energy 9 (2024) 1438–1447, https://doi.org/10.1038/s41560-024-01620-9.

[4] A. Geslin, L. Xu, D. Ganapathi, K. Moy, W.C. Chueh, S. Onori, Dynamic cycling enhances battery lifetime, Nat. Energy (2024), https://doi.org/10.1038/s41560-024-01675-8.

[5] F. Duffner, M. Wentker, M. Greenwood, J. Leker, Battery cost modeling: a review and directions for future research, Renew. Sustain. Energy Rev. 127 (2020) 109872, https://doi.org/10.1016/j.rser.2020.109872.

[6] Z. Wang, D. Shi, J. Zhao, Z. Chu, D. Guo, C. Eze, X. Qu, Y. Lian, A.F. Burke, Battery health diagnostics: bridging the gap between academia and industry, eTransportation 19 (2024) 100309, https://doi.org/10.1016/j.etran.2023.100309.

[7] S. Tao, M. Zhang, Z. Zhao, H. Li, R. Ma, Y. Che, X. Sun, L. Su, C. Sun, X. Chen, H. Chang, S. Zhou, Z. Li, H. Lin, Y. Liu, W. Yu, Z. Xu, H. Hao, S. Moura, X. Zhang, Y. Li, X. Hu, G. Zhou, Non-destructive degradation pattern decoupling for early battery trajectory prediction *via* physics-informed learning, Energy Environ. Sci. (2025), https://doi.org/10.1039/D4EE03839H, 10.1039.D4EE03839H.

[8] H. Liu, C. Li, X. Hu, J. Li, K. Zhang, Y. Xie, R. Wu, Z. Song, Multi-modal framework for battery state of health evaluation using open-source electric vehicle data, Nat. Commun. 16 (2025) 1137, https://doi.org/10.1038/s41467-025-56485-7.

[9] S. Tao, H. Liu, C. Sun, H. Ji, G. Ji, Z. Han, R. Gao, J. Ma, R. Ma, Y. Chen, S. Fu, Y. Wang, Y. Sun, Y. Rong, X. Zhang, G. Zhou, H. Sun, Collaborative and privacy-preserving retired battery sorting for profitable direct recycling via federated machine learning, Nat. Commun. 14 (2023) 8032, https://doi.org/10.1038/s41467-023-43883-y.

[10] S. Tao, R. Ma, Z. Zhao, G. Ma, L. Su, H. Chang, Y. Chen, H. Liu, Z. Liang, T. Cao, H. Ji, Z. Han, M. Lu, H. Yang, Z. Wen, J. Yao, R. Yu, G. Wei, Y. Li, X. Zhang, T. Xu, G. Zhou, Generative learning assisted state-of-health estimation for sustainable battery recycling with random retirement conditions, Nat. Commun. 15 (2024) 10154, https://doi.org/10.1038/s41467-024-54454-0.

[11] J. Zhu, Y. Wang, Y. Huang, R. Bhushan Gopaluni, Y. Cao, M. Heere, M. J. Mühlbauer, L. Mereacre, H. Dai, X. Liu, A. Senyshyn, X. Wei, M. Knapp, H. Ehrenberg, Data-driven capacity estimation of commercial lithium-ion batteries from voltage relaxation, Nat. Commun. 13 (2022) 2261, https://doi.org/10.1038/s41467-022-29837-w.

[12] Y. Ren, X. Sun, P. Wolfram, S. Zhao, X. Tang, Y. Kang, D. Zhao, X. Zheng, Hidden delays of climate mitigation benefits in the race for electric vehicle deployment, Nat. Commun. 14 (2023) 3164, https://doi.org/10.1038/s41467-023-38182-5.

[13] N. He, Q. Wang, Z. Lu, Y. Chai, F. Yang, Early prediction of battery lifetime based on graphical features and convolutional neural networks, Appl. Energy 353 (2024) 122048, https://doi.org/10.1016/j.apenergy.2023.122048.

[14] X. Han, L. Lu, Y. Zheng, X. Feng, Z. Li, J. Li, M. Ouyang, A review on the key issues of the lithium ion battery degradation among the whole life cycle, eTransportation 1 (2019) 100005, https://doi.org/10.1016/j.etran.2019.100005.

[15] R. Xiong, Y. Sun, C. Wang, J. Tian, X. Chen, H. Li, Q. Zhang, A data-driven method for extracting aging features to accurately predict the battery health, Energy Storage Mater. 57 (2023) 460–470, https://doi.org/10.1016/j.ensm.2023.02.034.

[16] H. Tian, P. Qin, K. Li, Z. Zhao, A review of the state of health for lithium-ion batteries: research status and suggestions, J. Clean. Prod. 261 (2020) 120813, https://doi.org/10.1016/j.jclepro.2020.120813.

[17] X. Han, S. Mao, Y. Wang, Y. Lu, D. Wang, Y. Sun, Y. Zheng, X. Feng, L. Lu, J. Hua, M. Ouyang, Manipulation of lithium dendrites based on electric field relaxation enabling safe and long-life lithium-ion batteries, Nat. Commun. 16 (2025), https://doi.org/10.1038/s41467-025-58818-y.

[18] M.B. Pinson, M.Z. Bazant, Theory of SEI formation in rechargeable batteries: capacity fade, accelerated aging and lifetime prediction, J. Electrochem. Soc. 160 (2013) A243–A250, https://doi.org/10.1149/2.044302jes.
[19] S. Yang, C. Zhang, J. Jiang, W. Zhang, L. Zhang, Y. Wang, Review on state-of-health of lithium-ion batteries: characterizations, estimations and applications, J. Clean. Prod. 314 (2021) 128015, https://doi.org/10.1016/j.jclepro.2021.128015.
[20] A. Fly, R. Chen, Rate dependency of incremental capacity analysis (dQ/dV) as a diagnostic tool for lithium-ion batteries, J. Energy Storage 29 (2020) 101329, https://doi.org/10.1016/j.est.2020.101329.
[21] R. Xiong, P. Wang, Y. Jia, W. Shen, F. Sun, Multi-factor aging in Lithium iron phosphate batteries: mechanisms and insights, Appl. Energy 382 (2025) 125250, https://doi.org/10.1016/j.apenergy.2024.125250.
[22] S. Tao, R. Guo, J. Lee, S. Moura, L.C. Casals, S. Jiang, J. Shi, S. Harris, T. Zhang, C. Y. Chung, G. Zhou, J. Tian, X. Zhang, Immediate remaining capacity estimation of heterogeneous second-life lithium-ion batteries *via* deep generative transfer learning, Energy Environ. Sci. (2025), https://doi.org/10.1039/d5ee02217g.
[23] J. Zhu, Data-Driven Capacity Estimation of Commercial lithium-ion Batteries from Voltage Relaxation, (n.d.).
[24] R. Ma, S. Tao, X. Sun, Y. Ren, C. Sun, G. Ji, J. Xu, X. Wang, X. Zhang, Q. Wu, G. Zhou, Pathway decisions for reuse and recycling of retired lithium-ion batteries considering economic and environmental functions, Nat. Commun. 15 (2024) 7641, https://doi.org/10.1038/s41467-024-52030-0.
[25] R. Li, N.D. Kirkaldy, F.F. Oehler, M. Marinescu, G.J. Offer, S.E.J. O'Kane, The importance of degradation mode analysis in parameterising lifetime prediction models of lithium-ion battery degradation, Nat. Commun. 16 (2025) 2776, https://doi.org/10.1038/s41467-025-57968-3.
[26] C. Liang, S. Tao, X. Huang, Y. Wang, B. Xia, X. Zhang, Stochastic state of health estimation for lithium-ion batteries with automated feature fusion using quantum convolutional neural network, J. Energy Chem. 106 (2025) 205–219, https://doi.org/10.1016/j.jechem.2025.02.030.
[27] T. Desai, A.J. Gallo, R.M.G. Ferrari, Multi timescale battery modeling: integrating physics insights to data-driven model, Appl. Energy 393 (2025) 126040, https://doi.org/10.1016/j.apenergy.2025.126040.
[28] S. Shen, M. Sadoughi, M. Li, Z. Wang, C. Hu, Deep convolutional neural networks with ensemble learning and transfer learning for capacity estimation of lithium-ion batteries, Appl. Energy 260 (2020) 114296, https://doi.org/10.1016/j.apenergy.2019.114296.
[29] J. Lu, R. Xiong, J. Tian, C. Wang, F. Sun, Deep learning to estimate lithium-ion battery state of health without additional degradation experiments, Nat. Commun. 14 (2023) 2760, https://doi.org/10.1038/s41467-023-38458-w.
[30] X. Huang, S. Tao, C. Liang, R. Ma, X. Wang, B. Xia, X. Zhang, Robust and generalizable lithium-ion battery health estimation using multi-scale field data decomposition and fusion, J. Power Sources 642 (2025) 236939, https://doi.org/10.1016/j.jpowsour.2025.236939.
[31] J. Tian, R. Xiong, W. Shen, J. Lu, F. Sun, Flexible battery state of health and state of charge estimation using partial charging data and deep learning, Energy Storage Mater. 51 (2022) 372–381, https://doi.org/10.1016/j.ensm.2022.06.053.
[32] K. Zheng, J. Meng, Z. Yang, F. Zhou, K. Yang, Z. Song, Refined lithium-ion battery state of health estimation with charging segment adjustment, Appl. Energy 375 (2024) 124077, https://doi.org/10.1016/j.apenergy.2024.124077.
[33] R. Liu, B. Jiang, A multi-time-resolution attention-based interaction network for co-estimation of multiple battery states, Appl. Energy 381 (2025) 125097, https://doi.org/10.1016/j.apenergy.2024.125097.
[34] G. Ma, S. Xu, B. Jiang, C. Cheng, X. Yang, Y. Shen, T. Yang, Y. Huang, H. Ding, Y. Yuan, Real-time personalized health status prediction of lithium-ion batteries using deep transfer learning, Energy Environ. Sci. 15 (2022) 4083–4094, https://doi.org/10.1039/D2EE01676A.
[35] R. Tan, X. Lu, M. Cheng, J. Li, J. Huang, T.-Y. Zhang, Forecasting battery degradation trajectory under domain shift with domain generalization, Energy Storage Mater. 72 (2024) 103725, https://doi.org/10.1016/j.ensm.2024.103725.
[36] Y. Che, X. Hu, X. Lin, J. Guo, R. Teodorescu, Health prognostics for lithium-ion batteries: mechanisms, methods, and prospects, Energy Environ. Sci. 16 (2023) 338–371, https://doi.org/10.1039/D2EE03019E.
[37] R. Tan, W. Hong, J. Tang, X. Lu, R. Ma, X. Zheng, J. Li, J. Huang, T.-Y. Zhang, BatteryLife: a comprehensive dataset and benchmark for battery life prediction. https://doi.org/10.48550/arXiv.2502.18807, 2025.
[38] H. Zhang, Y. Li, S. Zheng, Z. Lu, X. Gui, W. Xu, J. Bian, Battery lifetime prediction across diverse ageing conditions with inter-cell deep learning, Nat. Mach. Intell. (2025), https://doi.org/10.1038/s42256-024-00972-x.
[39] C. Szegedy, Wei Liu, Yangqing Jia, P. Sermanet, S. Reed, D. Anguelov, D. Erhan, V. Vanhoucke, A. Rabinovich, Going deeper with convolutions, in: 2015 IEEE Conference on Computer Vision and Pattern Recognition (CVPR), IEEE, Boston, MA, USA, 2015, pp. 1–9, https://doi.org/10.1109/cvpr.2015.7298594.
[40] J. Wang, J. Purewal, P. Liu, J. Hicks-Garner, S. Soukazian, E. Sherman, A. Sorenson, L. Vu, H. Tataria, M.W. Verbrugge, Degradation of lithium ion batteries employing graphite negatives and nickel–cobalt–manganese oxide + spinel manganese oxide positives: part 1, aging mechanisms and life estimation, J. Power Sources 269 (2014) 937–948, https://doi.org/10.1016/j.jpowsour.2014.07.030.
[41] C.R. Birkl, M.R. Roberts, E. McTurk, P.G. Bruce, D.A. Howey, Degradation diagnostics for lithium ion cells, J. Power Sources 341 (2017) 373–386, https://doi.org/10.1016/j.jpowsour.2016.12.011.
[42] J. Huang, S.T. Boles, J.-M. Tarascon, Sensing as the key to battery lifetime and sustainability, Nat. Sustain. 5 (2022) 194–204, https://doi.org/10.1038/s41893-022-00859-y.